ACS NANO

www.acsnano.org

ARTICLE

Spin-Polarized Tunneling through Chemical Vapor Deposited Multilayer Molybdenum Disulfide

André Dankert,[*,†] Parham Pashaei,[†] M. Venkata Kamalakar,[†,‡] Anand P. S. Gaur,[§,∥] Satyaprakash Sahoo,[*,§,⊥] Ivan Rungger,[#] Awadhesh Narayan,[¶,□] Kapildeb Dolui,[¶,△] Md. Anamul Hoque,[†] Ram Shanker Patel,[▽] Michel P. de Jong,[○] Ram S. Katiyar,[§] Stefano Sanvito,[*,¶] and Saroj P. Dash[*,†]

[†]Department of Microtechnology and Nanoscience, Chalmers University of Technology, SE-41296, Göteborg, Sweden

[‡]Department of Physics and Astronomy, Uppsala University, Box 516, 75120, Uppsala, Sweden

[§]Department of Physics and Institute for Functional Nanomaterials, University of Puerto Rico, San Juan, PR 00931, United States

[∥]Mechanical Engineering Department, Iowa State University, Ames, Iowa 50011, United States

[⊥]Institute of Physics, Bhubaneswar, Odisha 751005, India

[#]National Physical Laboratory, Teddington, TW11 0LW, United Kingdom

[¶]School of Physics, AMBER and CRANN Institute, Trinity College, Dublin 2, Ireland

[□]Materials Theory, ETH Zurich, Wolfgang-Pauli-Strasse 27, CH 8093, Zurich, Switzerland

[△]Department of Physics and Astronomy, University of Delaware, Newark, Delaware 19716-2570, United States

[▽]Department of Physics, Birla Institute of Technology and Science, Pilani - K K Birla Goa Campus, Zuarinagar, 403726, Goa, India

[○]MESA+ Institute for Nanotechnology University of Twente, 7500 AE Enschede, The Netherlands

S *Supporting Information*

ABSTRACT: **The two-dimensional (2D) semiconductor molybdenum disulfide (MoS_2) has attracted widespread attention for its extraordinary electrical-, optical-, spin-, and valley-related properties. Here, we report on spin-polarized tunneling through chemical vapor deposited multilayer MoS_2 (~7 nm) at room temperature in a vertically fabricated spin-valve device. A tunnel magnetoresistance (TMR) of 0.5−2% has been observed, corresponding to spin polarization of 5−10% in the measured temperature range of 300−75 K. First-principles calculations for ideal junctions result in a TMR up to 8% and a spin polarization of 26%. The detailed measurements at different temperature, bias voltages, and density functional theory calculations provide information about spin transport mechanisms in vertical multilayer MoS_2 spin-valve devices. These findings form a platform for exploring spin functionalities in 2D semiconductors and understanding the basic phenomena that control their performance.**

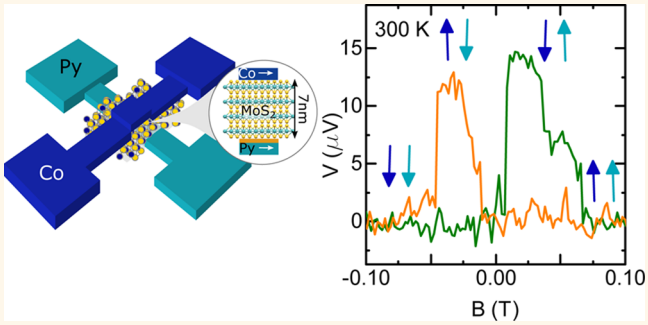

KEYWORDS: *spin-polarized tunneling, multilayer MoS_2, 2D semiconductor, tunnel magnetoresistance, density functional theory*

Spintronics is an emerging field for "beyond-CMOS" technology, where information is carried by spin instead of charge.[1] One of the primary challenges in this field is to discover semiconductor materials with functional spintronics properties.[2−4] Two dimensional (2D) crystals offer a unique potential for spintronic devices due to remarkable properties such as long spin-coherence lengths,[5,6] spin-polarized tunneling,[7,8] high spin−orbit coupling (SOC),[9] and spin-momentum locking.[10,11] Recently, long spin-coherence length in graphene has been achieved, due to its low SOC strengths and high mobility.[6,12,13] At the same time, atomically thin molybdenum disulfide (MoS_2)[14] has emerged as a promising semiconducting 2D crystal, demonstrating excellent electronic, optoelectronic, and spintronic properties. In monolayer MoS_2, the lack of

Received: April 24, 2017
Accepted: May 22, 2017
Published: May 30, 2017

DOI: 10.1021/acsnano.7b02819
ACS Nano 2017, 11, 6389−6395

inversion symmetry coupled to the high spin−orbit interaction leads to a unique spin and valley polarization.[15] Recently, nanosecond electron spin lifetimes have been observed in MoS_2 at low temperatures, by using optical Kerr spectroscopy experiments[16] and spin-valve measurements.[17] The high SOC of MoS_2[18] has also been exploited for proximity-induced effects,[18−21] switching of spin current,[22,23] and control of spin lifetime[23] in graphene heterostructure channels up to room temperature.[23]

In order to further explore the spintronic properties of MoS_2, the investigation of spin transport in a vertical magnetic tunnel junction (MTJ) is an interesting approach, where the transport channel is defined by a few-nanometer-thick MoS_2 spacer sandwiched between two ferromagnetic (FM) electrodes. Employing such MTJs, a unique spin filtering effect was theoretically predicted for some 2D materials and first observed in graphene/graphite-based devices.[24−27] Beyond graphene, it is interesting to investigate whether similar spin filtering effects may be observed for MTJs based on insulating or semiconducting 2D crystals. Recently, insulating hexagonal boron nitride (h-BN) tunnel barriers have been used showing excellent spin-polarized tunneling and filtering properties.[28,29,7,8] Since h-BN binds little to the metallic surfaces, it is interesting to fabricate MTJs with other layered compounds likely to be more reactive with the magnetic electrodes. This is for instance the case of MoS_2, since it was predicted that semiconducting multilayer MoS_2 junctions can exhibit a large tunnel magnetoresistance (TMR) up to 300% in the tunneling regime.[30] Recently, *ab initio* calculations and experiments have shown that monolayer MoS_2 and WS_2 MTJs are metallic due to strong coupling between the Fe and the S atoms at the interface, showing a magnetoresistance of ∼0.5%.[31−33] However, MTJs incorporating multilayer MoS_2 with semiconducting properties are expected to show enhanced performance. Such multilayer MoS_2 MTJs and room-temperature operation have not been realized experimentally so far. Moreover, the possibility of using large-scale multilayer MoS_2 can further enhance the impact of such devices for practical applications.

Considering the potential impact of 2D semiconductor MTJs, here we report on spin-polarized tunneling through a chemical vapor deposition (CVD)-grown multilayer MoS_2 in a spin-valve structure, measuring a TMR up to room temperature. Specifically, we have employed vertical spin-valve devices, with 7 nm thick MoS_2 sandwiched between two FM electrodes. A TMR up to 2% is observed when the magnetic alignment of the two electrodes is switched from parallel to antiparallel due to the transmission of spin-polarized electrons through the multilayer MoS_2 spacer. By combining bias- and temperature-dependent TMR measurements with density functional theory calculations, we bring out the detailed information about the spin polarization at the interfaces and the spin transport process through the multilayer MoS_2 junctions.

RESULTS AND DISCUSSION

Tunneling magnetoresistance is a consequence of the spin-dependent tunneling in magnetic tunnel junctions with a MoS_2 barrier as shown in Figure 1a. The device geometry shown in Figure 1b incorporates a 7 nm thick MoS_2 layer sandwiched between two FMs in a vertical structure. Specifically, the devices consist of a $Ni_{80}Fe_{20}$ (30 nm)/AlO_x(0.8 nm)/MoS_2(7 nm)/Co(50 nm) stack, fabricated using photolithography, metal evaporation, and 2D layer transfer techniques (see

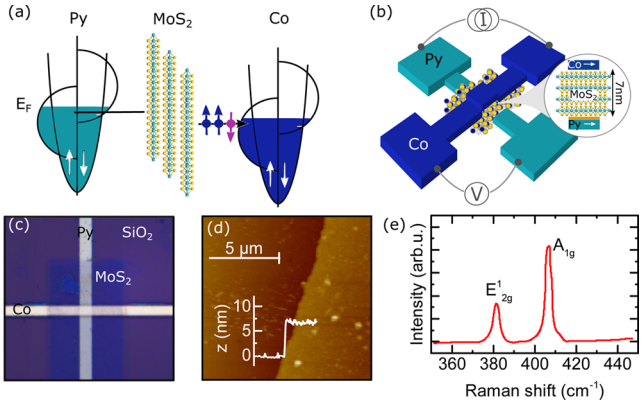

Figure 1. Multilayer MoS_2 tunnel magnetoresistance device. (a) Spin-dependent tunneling in magnetic tunnel junctions with a multilayer MoS_2 barrier. (b) Schematic representation of the multilayer MoS_2 vertical device with ferromagnetic contacts and a MoS_2 spacer. The measurement scheme is shown with four-probe cross-bar geometry. (c) Optical microscope image of a fabricated device consisting of a large-area CVD-grown multilayer MoS_2 junction of 7 nm thickness and ferromagnetic Co and $Ni_{80}Fe_{20}$(Py)/AlO_x (0.8 nm) contacts as top and bottom electrodes, respectively. The active junction area is 5 × 20 μm^2. (d) Atomic force microscope scan of 7 nm CVD MoS_2 on a SiO_2/Si substrate. (e) Raman spectra of 7 nm CVD MoS_2 measured at room temperature.

Methods). The thin AlO_x layer was prepared by Al evaporation and a natural oxidation. This AlO_x layer is expected to protect the bottom $Ni_{80}Fe_{20}$ electrode from oxidation and acts as a leaky tunnel barrier.[34] An optical microscope image of a fabricated MoS_2 vertical device is shown in Figure 1c. The multilayer MoS_2 chosen in our devices is grown over a large area on a SiO_2/Si substrate by the CVD method in optimized growth conditions.[35] The thickness of the MoS_2 layer is determined to be 7 nm by AFM measurement, as shown in Figure 1d, which corresponds to around 10 monolayers (one monolayer around 6.5 Å). Figure 1e shows the Raman spectrum of a MoS_2 film displaying the two Raman-active modes at ∼384 cm^{-1} (E^1_{2g}) and ∼407 cm^{-1} (A_{1g}) at room temperature.

The electrical transport properties of our junctions are measured in four-terminal geometry as displayed in Figure 1b. We observe increasingly nonlinear current−voltage (I−V) characteristics of the junction at lower temperatures (Figure 2a). Figure 2b displays the normalized junction resistance ($R = V/I$) as a function of temperature (T), where the R value doubles upon cooling from 300 K to 75 K. Such a large variation is expected due to the presence of a MoS_2 semiconducting barrier in the junction, whereas insulating Al_2O_3 barriers usually show an increase in R of 10−20% in the same range.[34] The strong temperature dependence observed here can be attributed to inelastic tunneling or gap-state-assisted tunneling through the MoS_2 layers.[36] In order to verify this behavior, the dI/dV and d^2I/dV^2 curves are plotted in Figure 2c and d, respectively.[37] The differential conductance $G = dI/dV$ *versus* bias voltage curves at both high and low temperatures are almost symmetric and linear, as shown in Figure 2c. Therefore, the transport through a 7 nm thick MoS_2 layer can be mainly attributed to tunneling in the measured bias range. The junctions are also found to be quite stable up to an applied bias of 200 mV and also do not exhibit any zero bias anomaly, suggesting the absence of magnetic impurities. Figure

DOI: 10.1021/acsnano.7b02819
ACS Nano 2017, 11, 6389−6395

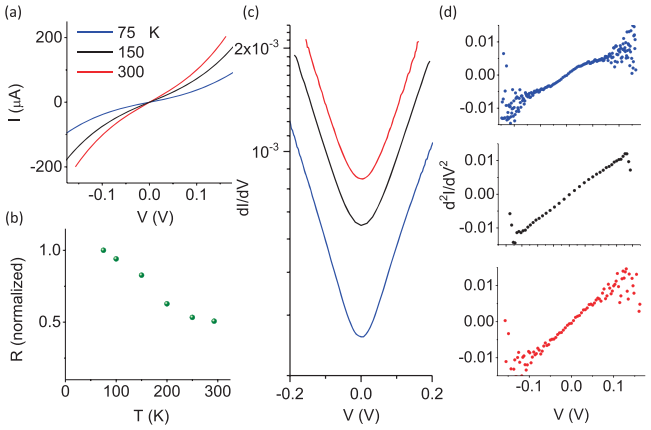

Figure 2. Electrical characterization of multilayer MoS_2 vertical devices. (a) Current−voltage (I−V) characteristics of the junction at the different temperatures of 75, 150, and 300 K. (b) Temperature dependence of the MoS_2 junction resistance (normalized) at a bias voltage of 5 mV. (c) Differential conductance (dI/dV) as a function of bias voltage at different temperatures. (d) Derivative of the differential conductance, d^2I/dV^2, for the same junction at three different temperatures.

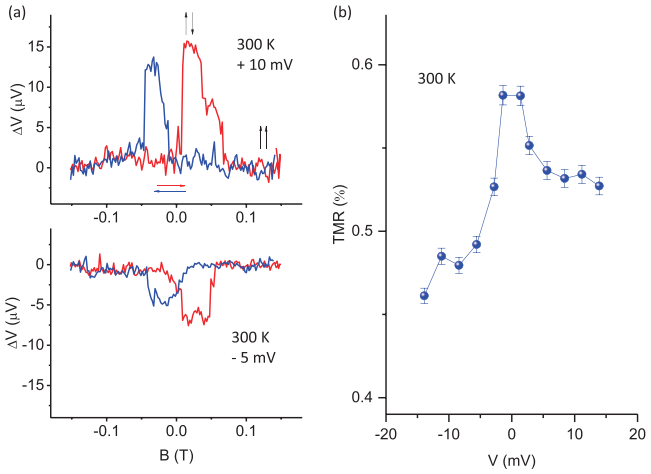

Figure 3. Spin-valve measurements in multilayer MoS_2 MTJs at room temperature. (a) Tunnel magnetoresistance (TMR) measurements on the device with an in-plane magnetic field B_{in} for applied bias voltages of +10 mV (upper panel) and −5 mV (lower panel) at room temperature (300 K). The arrows indicate the up (red) and down (blue) B field sweep directions. (b) Bias dependence of TMR signal measured at 300 K.

2d shows the derivative of G (d^2I/dV^2) as a function of bias voltage at different temperatures. At 75 K, two distinct conduction regions can be observed, as indicated by change in the slope of the curves. Above $V = \pm 50$ mV an extra conducting channel is opening up, consistent with the appearance of inelastic scattering events. In contrast, for 150 and 300 K already at low bias this high conducting channel is established.

The junction resistance for thick MoS_2 (7 nm) consists of both the interlayer and intralayer resistances. The couplings between the 2D MoS_2 layers are expected to arise from the overlap of the electron wave functions due to the small separation between the sulfide layers, with a charge screening length of ∼7 nm.[38] This is explicitly distinct from the current spreading in multilayer graphene with a limited charge screening length of only 0.6 nm.[39] The characteristics arise due to the transport involving the d-electrons of MoS_2, while the p_z-orbitals are contributing in graphene. For thinner MoS_2 layers (few monolayers) a direct tunneling dominates, with the tunneling conductance exponentially decreasing with increasing MoS_2 thickness.[40−42] However, for thicker samples used in the present study, inelastic tunneling or gap-state-assisted tunneling through defects in the form of S-vacancies cannot be ruled out at low temperatures.[36]

Next, we performed magnetoresistance measurements with 7 nm multilayer MoS_2 MTJs by applying a fixed bias current while measuring the voltage drop as a function of the external in-plane magnetic field, B. The TMR across the MoS_2 junction is observed at room temperature as a difference in the resistances measured for the parallel, R_p, and antiparallel, R_{ap}, alignment of the magnetizations of the FM electrodes, as shown in Figure 3a. The well-defined resistance states R_p and R_{ap} are achieved by using different FM materials (Co and NiFe) and electrode widths on either side of the MoS_2 layer. The measured magneto voltage signal of $\Delta V = 15$ μV corresponds to a TMR $= \frac{R_p - R_{ap}}{R_p} \times 100\% = 0.5\%$ at 300 K. We estimate the spin polarization of the contacts from the Julliere relation TMR $= \frac{2P_1P_2}{1 - P_1P_2}$,[43,44] resulting in $P_1 = P_2 = 5\%$ (assuming the polarizations of Co and $Ni_{80}Fe_{20}$ to be similar). We would like to note that the spin polarization obtained with introduction of MoS_2 is smaller than the polarization of ferromagnetic tunnel contacts reported in the literature.[44] This can be attributed to disorder introduced at the interfaces during the wet transfer process of the CVD MoS_2 layer onto the ferromagnetic electrode. It has also to be noted that the spin transport process is very sensitive to defect-assisted tunneling (*i.e.*, multistep tunneling) through MoS_2 and can significantly affect the TMR.[45] This can cause additional spin flip scattering due to the presence of strong spin−orbit coupling in MoS_2.[46] As predicted theoretically, the spin polarization is expected to be higher with development of an all *in situ* method for preparation of good-quality MoS_2 layers and ferromagnetic tunnel contacts. However, our effort to integrate a ferromagnetic tunnel junction to CVD MoS_2 in an *ex situ* fabrication process shows promising results with a TMR up to room temperature. We reproduced the TMR measurements on several devices with MoS_2 junctions on different chips prepared by similar fabrication methods. The resistance−area (RA) products measured on different devices vary from 7.5 to 25 kΩ·μm^2, giving rise to variations of TMR from 0.2% to 0.5% at room temperature. In the Supporting Information Figure S1, we present TMR measurements and bias dependence of another set of such devices at room temperature.

Even though the observation of a TMR offers evidence for spin-polarized transport, a careful investigation of the bias and temperature dependence is essential for a physical understanding of the phenomenon. The applications of negative and positive bias voltages correspond to a spin transport through the MoS_2 from $Ni_{80}Fe_{20}$ to Co and Co to $Ni_{80}Fe_{20}$, respectively. The bias dependence of the TMR signal changes sign with reversing bias polarity (shown in Figure 3a). The bias dependence of the absolute value of TMR at room temperature measured at different voltages across the junction is shown in Figure 3b. We observe a decrease of the TMR at higher bias voltages with a maximum around zero bias voltage. Such behavior can be attributed to the excitation of magnons, to band bending, and possibly to the involvement of interface

DOI: 10.1021/acsnano.7b02819
ACS Nano 2017, 11, 6389−6395

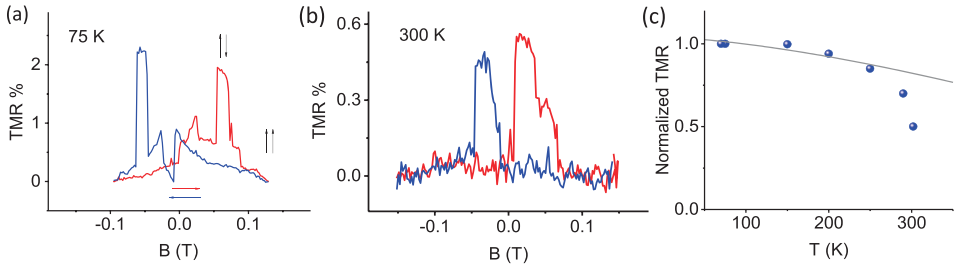

Figure 4. Temperature dependence of TMR in multilayer MoS_2 MTJ. (a) Tunnel magnetoresistance (TMR) measurements at 75 K. (b) TMR measured at 300 K. The arrows indicate the up and down *B* field sweep directions. (c) Temperature dependence of the TMR signal (normalized). The fitting represents the temperature dependence of TMR α $1 - \alpha T^{3/2}$.

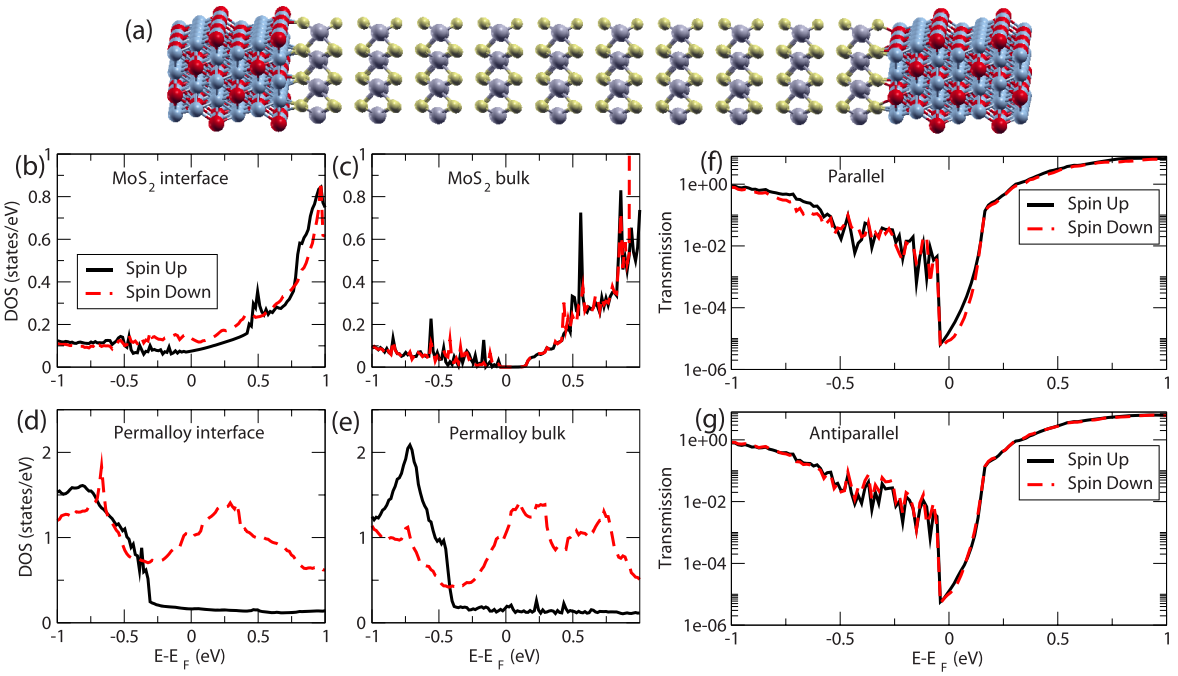

Figure 5. Theoretical results for a permalloy/MoS_2/permalloy junction. (a) Junction setup for transport calculations with 10 layers of MoS_2, corresponding to a barrier thickness of about 6.4 nm, sandwiched between semi-infinite permalloy ($Ni_{80}Fe_{20}$) electrodes. Density of states (DOS) as a function of energy for the (b) interface MoS_2 layer, (c) MoS_2 layer in the bulk of the spacer, (d) interface permalloy layer, and (e) bulk permalloy. Spin-resolved transmission (f) for parallel and (g) antiparallel configurations of the junction.

states at high voltages, as also observed in other material systems.[37] The bias dependence is also found to be asymmetric with polarity, decreasing much faster in the negative than the positive bias range. This behavior can be due to asymmetric barrier interfaces (Co/MoS_2 and $Ni_{80}Fe_{20}/AlO_x/MoS_2$) at the two sides of the MoS_2 layer. Similar bias dependence behavior has also been observed in some cases in other magnetic tunnel junctions with inorganic and organic semiconductors[47] and tunnel junctions with Al_2O_3, MgO, and h-BN.[48,49,29]

In order to investigate the details of the spin transport process through MoS_2, spin-valve measurements were performed at different temperatures. The TMR shows an overall increase up to 2% at 75 K, corresponding to a spin polarization of 10% (as extracted from Julliere's formula[43]). Figure 4a shows the TMR at 75 and 300 K, and the normalized TMR as a function of temperature is plotted in Figure 4b. We model the observed TMR decrease with increasing temperature by considering the spin polarization to have the same temperature dependence of the surface magnetization, which is described by the spin wave excitation model with a $T^{3/2}$ temperature dependence.[50] We observe a faster decrease of the TMR at higher temperatures, in comparison to the expected moderate decrease. Although such behavior is not well understood, in general it can be attributed to a lower Curie temperature (T_c) of the ferromagnetic electrodes and also to the low barrier height of the multilayer MoS_2 junction.

In order to further understand the transport properties of the devices, we have carried out density functional theory based transport calculations for an ideal, defect-free junction (see Computational Methods for details). The setup for our computations is shown in Figure 5a for a junction made of 10 MoS_2 layers sandwiched between two semi-infinite permalloy ($Ni_{80}Fe_{20}$) electrodes. Note that we use permalloy for both electrodes, which is a reasonable approximation since the Co density of states (DOS) is rather similar to that of permalloy.[51] The use of an approximately symmetric setup is also justified by the rather small asymmetry found in the experimental *I*−*V* and TMR−*V* curves. The spin-resolved DOS projected onto different layers of the junction is shown in Figure 5b−e. We find that the MoS_2 interface layer becomes

DOI: 10.1021/acsnano.7b02819
ACS Nano 2017, 11, 6389−6395

metallic due to a strong hybridization with permalloy, similar to what has been found for single-layer MoS_2.[31] In contrast, as one moves into the bulk of the spacer, a gap reminiscent of pristine MoS_2 emerges. Notably, the DOS at the Fermi level of the interface MoS_2 layer becomes spin polarized, which indicates spin injection into MoS_2. Considering the first MoS_2 layer as the effective metallic interface layer, we find the theoretical upper limit to the efficiency for spin injection in this junction, as $\eta = (DOS_\downarrow - DOS_\uparrow)/(DOS_\downarrow + DOS_\uparrow) \approx 26\%$. This number is significantly smaller than the value in the bulk permalloy (73%) and at the permalloy interface layer (76%).

The spin-resolved transmission as a function of energy for the parallel and antiparallel configurations is plotted in Figure 5f and g, respectively. At the Fermi level, we find MR = $(T_{parallel} - T_{antiparallel})/T_{antiparallel} \approx 8\%$. Furthermore, we have evaluated the MR for different thicknesses of MoS_2 (6.4, 8.8, and 11.1 nm) by adding additional layers in the junction. We have obtained MR values ranging between 8.6% and 10.7%, showing that there is no significant change with thickness. This indicates that the MR is driven by the interface polarization rather than the symmetry driven length- and *k*-dependent spin-filtering like in epitaxial and crystalline Fe(100)/MgO/Fe tunnel junctions.[30] The important conclusion for MoS_2-based junctions is that, since in general the interface between the 2D material and the electrode is not epitaxial and requires a rather large supercell to simulate, there is no well-defined symmetry of such interface. As a consequence all the effects based on the symmetry of the interface are not relevant anymore, so that symmetry does not lead to spin filtering. Furthermore, a large supercell in the plane leads to a small Brillouin zone in *k*-space. Since the range of independent *k*-points is therefore restricted to a small area around the Γ-point, also the *k*-dependent spin-filtering is suppressed.[30] The remaining MR can therefore only originate from the different spin polarization at the metal/insulator interfaces, as described by Julliere's model, and leads to a thickness-independent MR.

This MR value, under ballistic transport conditions for an ideal tunnel junction, should be considered as an upper limit to the MR for devices with permalloy electrodes. However, the presence of defects in MoS_2, as well as inelastic scattering processes, can reduce the spin polarization of the current, thereby reducing the magnetoresistance down to the experimentally measured values. The MR obtained here is rather similar to that of a single MoS_2 layer with permalloy electrodes[31] and lower than theoretical predictions for multilayer MoS_2 junctions with Fe electrodes.[30] The origin of the reduced MR lies in the reduced polarization and spin filtering induced by the permalloy electrodes when compared to Fe electrodes, which also have a better lattice match with MoS_2. This observation also shows that the choice of electrode materials and lattice matching are crucial factors in obtaining high magnetoresistance in MoS_2-based tunnel junctions.

CONCLUSIONS

In summary, we have demonstrated spin-polarized tunneling in multilayer MoS_2 at room temperature in a vertical spin-valve device. The spin-transport through 7 nm of MoS_2 produces a TMR of 0.5% at room temperature, which shows enhancement up to 2% at 75 K, corresponding to an increase of spin polarization from 5% to 10%. Our density functional theory based transport calculations for ideal spin valves provide an upper limit to the TMR of 8%, while the maximum spin polarization is obtained to be 26%. The theoretical results also show that interfaces without epitaxial growth generally lead to rather low MR ratios when compared to junctions with better lattice match across the layers. The lower experimentally obtained spin polarization possibly can be attributed to interface contamination during the transfer process, defect-assisted tunneling, and spin-flip scattering due to spin−orbit coupling in MoS_2. These results on vertical spin transport in large-area multilayer MoS_2 reveal useful information needed for the development of 2D semiconductor materials and their heterostructures for spintronic devices.

METHODS

Materials Growth and Characterization. We fabricated the MoS_2/ferromagnetic metal heterostructures using MoS_2 films grown by chemical vapor deposition. The large-area MoS_2 films were synthesized on SiO_2/Si substrates *via* CVD and sulfurization of molybdenum films at 900 °C. The film thickness was characterized in tapping mode atomic force microscopy (AFM-VEECO). Raman and photoluminescence spectroscopy were carried out using a Horiba-Jobin T64000 (triple mode subtractive) micro-Raman system in backscattering configuration utilizing an argon ion laser (514.5 nm line as excitation source).

Device Fabrication. Spin transport devices incorporating a multilayer MoS_2 between two FM metal electrodes in a vertical geometry were fabricated. The bottom $Ni_{80}Fe_{20}$ (30 nm) electrodes were prepared on a Si/SiO_2 substrate by photolithography, electron beam evaporation, and lift-off methods. Before deposition of $Ni_{80}Fe_{20}$ electrodes, we deposited a thin layer of Ti in order to increase adhesion of FM to the SiO_2 substrate. The bottom $Ni_{80}Fe_{20}$ electrodes were capped with 0.8 nm of Al and subsequently oxidized naturally to make an AlO_x layer, which should protect the bottom ferromagnet $Ni_{80}Fe_{20}$ from oxidation and contamination during transfer of MoS_2.

The large-area MoS_2 films grown on the SiO_2 substrate were first covered with a poly(methyl methacrylate) (PMMA) layer and then released from the substrate by etching in KOH. After a deionized water rinse, the MoS_2/PMMA layer was transferred onto the bottom $Ni_{80}Fe_{20}$ electrodes. After drying the chip in an ambient environment, we annealed it at 150 °C for 10 min. It has been observed that this annealing step improved adhesion of MoS_2 with the bottom $Ni_{80}Fe_{20}$ electrode. The chip was then cleaned with acetone to remove the PMMA. The active device areas of the MoS_2 layer were patterned by lithography and Ar ion beam etching with the SIMS etch stop technique. The top Co (65 nm) electrodes and capping Au (20 nm) layer were prepared by photolithography, electron beam evaporation, and lift-off techniques in a cross-bar geometry. The final device consisted of junctions with $Ni_{80}Fe_{20}$ (30 nm)/AlO_x (0.8 nm)/MoS_2 (7 nm)/Co (65 nm) heterostructures.

Computational Methods. *Ab initio* transport calculations were performed using the Smeagol package.[52−54] The code interfaces the nonequilibrium Green's function method for transport with density functional theory, as implemented in the SIESTA code.[55] Norm-conserving pseudopotentials were used to replace the core electrons, and a double-ζ polarized basis set was employed, along with a mesh cutoff of 300 Ry. The local density approximation to the exchange−correlation functional was used.[56] An in-plane supercell of dimensions 14.37 Å × 8.29 Å was constructed, with the total length of the scattering region along the transport direction being 82.65 Å. Periodic boundary conditions were implemented perpendicular to the transport direction, with a 2 × 4 *k*-point mesh sampling used for the self-consistent calculations. Transmission coefficients and densities of states were obtained for the so-converged charge density by integrating over a denser 10 × 20 *k*-point grid.

ASSOCIATED CONTENT

Supporting Information

The Supporting Information is available free of charge on the ACS Publications website at DOI: 10.1021/acsnano.7b02819.

DOI: 10.1021/acsnano.7b02819
ACS Nano 2017, 11, 6389−6395

Reproducibility of devices with measurement of TMR and its bias dependence at room temperature (PDF)

AUTHOR INFORMATION

Corresponding Authors

*E-mail: andre.dankert@chalmers.se.
*E-mail: sahoo@iopb.res.in.
*E-mail: stefano.sanvito@tcd.ie.
*E-mail: saroj.dash@chalmers.se.

ORCID

André Dankert: 0000-0002-8024-3525
Ram Shanker Patel: 0000-0003-3532-3961
Saroj P. Dash: 0000-0001-7931-4843

Notes

The authors declare no competing financial interest.

ACKNOWLEDGMENTS

S.P.D. acknowledges financial support from EU Graphene Flagship (No. 604391), EU FlagEra project (from Swedish Research council VR No. 2015-06813), Swedish Research Council VR project grants (No. 2016-03658), and Graphene Center and the AoA Nano Program at Chalmers University of Technology. R.K. acknowledges financial support from DOE (Grant No. DEG02-ER46526) and a stipend to A.P.S.G. S. Sahoo acknowledges receiving financial support as PDF through NSF Grant EPS-01002410. R.S.P. acknowledges the financial support from Department of Science and Technology, Government of India, through the Nanomission Program (No. SR/NM/MS-1002/2010). S. Sanvito thanks Science Foundation Ireland (Grant No. 14/IA/2624) for financial support. I.R. thanks the European Union for financial support through the FP7 project ACMOL (Grant No. 618082).

REFERENCES

(1) Žutić, I.; Fabian, J.; Das Sarma, S. Spintronics: Fundamentals and Applications. *Rev. Mod. Phys.* **2004**, *76*, 323−410.
(2) Awschalom, D. D.; Flatté, M. E. Challenges for Semiconductor Spintronics. *Nat. Phys.* **2007**, *3*, 153−159.
(3) Dash, S. P.; Sharma, S.; Patel, R. S.; de Jong, M. P.; Jansen, R. Electrical Creation of Spin Polarization in Silicon at Room Temperature. *Nature* **2009**, *462*, 491−494.
(4) Roche, S.; Åkerman, J.; Beschoten, B.; Charlier, J.-C.; Chshiev, M.; Dash, S. P.; Dlubak, B.; Fabian, J.; Fert, A.; Guimarães, M.; et al. Graphene Spintronics: The European Flagship Perspective. *2D Mater.* **2015**, *2*, 30202.
(5) Tombros, N.; Jozsa, C.; Popinciuc, M.; Jonkman, H. T.; van Wees, B. J. Electronic Spin Transport and Spin Precession in Single Graphene Layers at Room Temperature. *Nature* **2007**, *448*, 571−574.
(6) Kamalakar, M. V.; Groenveld, C.; Dankert, A.; Dash, S. P. Long Distance Spin Communication in Chemical Vapour Deposited Graphene. *Nat. Commun.* **2015**, *6*, 6766.
(7) Kamalakar, M. V.; Dankert, A.; Bergsten, J.; Ive, T.; Dash, S. P. Enhanced Tunnel Spin Injection into Graphene Using Chemical Vapor Deposited Hexagonal Boron Nitride. *Sci. Rep.* **2015**, *4*, 6146.
(8) Kamalakar, M. V.; Dankert, A.; Kelly, P. J.; Dash, S. P. Inversion of Spin Signal and Spin Filtering in Ferromagnet|Hexagonal Boron Nitride-Graphene van Der Waals Heterostructures. *Sci. Rep.* **2016**, *6*, 21168.
(9) Gong, Z.; Liu, G.-B.; Yu, H.; Xiao, D.; Cui, X.; Xu, X.; Yao, W. Magnetoelectric Effects and Valley-Controlled Spin Quantum Gates in Transition Metal Dichalcogenide Bilayers. *Nat. Commun.* **2013**, *4*, 2053.
(10) Li, C. H.; van 't Erve, O. M. J.; Robinson, J. T.; Liu, Y.; Li, L.; Jonker, B. T. Electrical Detection of Charge-Current-Induced Spin Polarization due to Spin-Momentum Locking in Bi2Se3. *Nat. Nanotechnol.* **2014**, *9*, 218−224.
(11) Dankert, A.; Geurs, J.; Kamalakar, M. V.; Charpentier, S.; Dash, S. P. Room Temperature Electrical Detection of Spin Polarized Currents in Topological Insulators. *Nano Lett.* **2015**, *15*, 7976−7981.
(12) Drögeler, M.; Franzen, C.; Volmer, F.; Pohlmann, T.; Banszerus, L.; Wolter, M.; Watanabe, K.; Taniguchi, T.; Stampfer, C.; Beschoten, B. Spin Lifetimes Exceeding 12 Ns in Graphene Nonlocal Spin Valve Devices. *Nano Lett.* **2016**, *16* (6), 3533−3539.
(13) Ingla-Aynés, J.; Guimarães, M. H. D.; Meijerink, R. J.; Zomer, P. J.; Van Wees, B. J. 24-μ M Spin Relaxation Length in Boron Nitride Encapsulated Bilayer Graphene. *Phys. Rev. B: Condens. Matter Mater. Phys.* **2015**, *92*, 201410.
(14) Dankert, A.; Langouche, L.; Kamalakar, M. V.; Dash, S. P. High-Performance Molybdenum Disulfide Field-Effect Transistors with Spin Tunnel Contacts. *ACS Nano* **2014**, *8*, 476−482.
(15) Xu, X.; Yao, W.; Xiao, D.; Heinz, T. F. Spin and Pseudospins in Layered Transition Metal Dichalcogenides. *Nat. Phys.* **2014**, *10*, 343−350.
(16) Yang, L.; Sinitsyn, N. a.; Chen, W.; Yuan, J.; Zhang, J.; Lou, J.; Crooker, S. A. Long-Lived Nanosecond Spin Relaxation and Spin Coherence of Electrons in Monolayer MoS2 and WS2. *Nat. Phys.* **2015**, *11*, 830−834.
(17) Liang, S.; Yang, H.; Renucci, P.; Tao, B.; Laczkowski, P.; Mc-Murtry, S.; Wang, G.; Marie, X.; George, J.-M.; Petit-Watelot, S.; Djeffal, A.; Mangin, S.; Jaffrès, H.; Lu, Y. Electrical Spin Injection and Detection in Molybdenum Disulfide Multilayer Channel. *Nat. Commun.* **2017**, *8*, 14947.
(18) Gmitra, M.; Fabian, J. Graphene on Transition-Metal Dichalcogenides: A Platform for Proximity Spin-Orbit Physics and Optospintronics. *Phys. Rev. B: Condens. Matter Mater. Phys.* **2015**, *92*.10.1103/PhysRevB.92.155403
(19) Avsar, A.; Tan, J. Y.; Taychatanapat, T.; Balakrishnan, J.; Koon, G. K. W.; Yeo, Y.; Lahiri, J.; Carvalho, A.; Rodin, a S.; O'Farrell, E. C. T.; Eda, G.; Castro Neto, A. H.; Özyilmaz, B. Spin−orbit Proximity Effect in Graphene. *Nat. Commun.* **2014**, *5*, 4875.
(20) Yang, B.; Tu, M.-F.; Kim, J.; Wu, Y.; Wang, H.; Alicea, J.; Wu, R.; Bockrath, M.; Shi, J. Tunable Spin-Orbit Coupling and Symmetry-Protected Edge States in graphene/WS_2. *2D Mater.* **2016**, *3*, 31011.
(21) Wang, Z.; Ki, D.-K.; Chen, H.; Berger, H.; MacDonald, A. H.; Morpurgo, A. F. Strong Interface-Induced Spin-Orbit Interaction in Graphene on WS2. *Nat. Commun.* **2015**, *6*, 8339.
(22) Yan, W.; Txoperena, O.; Llopis, R.; Dery, H.; Hueso, L. E.; Casanova, F. A Two-Dimensional Spin Field-Effect Switch. *Nat. Commun.* **2016**, *7*, 13372.
(23) Dankert, A.; Dash, S. P. All-Electrical Spin Field Effect Transistor in van Der Waals Heterostructures at Room Temperature. arXiv:1610.06326, 2016.
(24) Karpan, V. M.; Giovannetti, G.; Khomyakov, P. A.; Talanana, M.; Starikov, A. A.; Zwierzycki, M.; Van Den Brink, J.; Brocks, G.; Kelly, P. J. Graphite and Graphene as Perfect Spin Filters. *Phys. Rev. Lett.* **2007**, *99*10.1103/PhysRevLett.99.176602.
(25) Cobas, E.; Friedman, A. L.; Van'T Erve, O. M. J.; Robinson, J. T.; Jonker, B. T. Graphene as a Tunnel Barrier: Graphene-Based Magnetic Tunnel Junctions. *Nano Lett.* **2012**, *12*, 3000−3004.
(26) Martin, M. B.; Dlubak, B.; Weatherup, R. S.; Yang, H.; Deranlot, C.; Bouzehouane, K.; Petroff, F.; Anane, A.; Hofmann, S.; Robertson, J.; Fert, A.; Seneor, P. Sub-Nanometer Atomic Layer Deposition for Spintronics in Magnetic Tunnel Junctions Based on Graphene Spin-Filtering Membranes. *ACS Nano* **2014**, *8*, 7890−7895.
(27) Iqbal, M. Z.; Iqbal, M. W.; Lee, J. H.; Kim, Y. S.; Chun, S. H.; Eom, J. Spin Valve Effect of NiFe/graphene/NiFe Junctions. *Nano Res.* **2013**, *6*, 373−380.
(28) Karpan, V. M.; Khomyakov, P. A.; Giovannetti, G.; Starikov, A. A.; Kelly, P. J. Ni(111)|graphene|h-BN Junctions as Ideal Spin Injectors. *Phys. Rev. B: Condens. Matter Mater. Phys.* **2011**, *84*, 153406.
(29) Dankert, A.; Kamalakar, M. V.; Wajid, A.; Patel, R. S.; Dash, S. P. Tunnel Magnetoresistance with Atomically Thin Two-Dimensional Hexagonal Boron Nitride Barriers. *Nano Res.* **2015**, *8*, 1357−1364.

DOI: 10.1021/acsnano.7b02819
ACS Nano 2017, 11, 6389−6395

(30) Dolui, K.; Narayan, A.; Rungger, I.; Sanvito, S. Efficient Spin Injection and Giant Magnetoresistance in Fe/MoS2/Fe Junctions. *Phys. Rev. B: Condens. Matter Mater. Phys.* **2014**, *90*, 041401.
(31) Wang, W.; Narayan, A.; Tang, L.; Dolui, K.; Liu, Y.; Yuan, X.; Jin, Y.; Wu, Y.; Rungger, I.; Sanvito, S.; Xiu, F. Spin-Valve Effect in NiFe/MoS2/NiFe Junctions. *Nano Lett.* **2015**, *15*, 5261−5267.
(32) Wu, H.-C.; Coileáin, C. Ó.; Abid, M.; Mauit, O.; Syrlybekov, A.; Khalid, A.; Xu, H.; Gatensby, R.; Jing Wang, J.; Liu, H.; Yang, L.; Duesberg, G. S.; Zhang, H.-Z.; Abid, M.; Shvets, I. V. Spin-Dependent Transport Properties of Fe3O4/MoS2/Fe3O4 Junctions. *Sci. Rep.* **2015**, *5*, 15984.
(33) Iqbal, M. Z.; Iqbal, M. W.; Siddique, S.; Khan, M. F.; Ramay, S. M. Room Temperature Spin Valve Effect in NiFe/WS2/Co Junctions. *Sci. Rep.* **2016**, *6*, 21038.
(34) Santos, T. S.; Lee, J. S.; Migdal, P.; Lekshmi, I. C.; Satpati, B.; Moodera, J. S. Room-Temperature Tunnel Magnetoresistance and Spin-Polarized Tunneling through an Organic Semiconductor Barrier. *Phys. Rev. Lett.* **2007**, *98*, 016601.
(35) Gaur, A. P. S.; Sahoo, S.; Ahmadi, M.; Dash, S. P.; Guinel, M. J. F.; Katiyar, R. S. Surface Energy Engineering for Tunable Wettability through Controlled Synthesis of MoS2. *Nano Lett.* **2014**, *14*, 4314−4321.
(36) Ahmed, F.; Choi, M. S.; Liu, X.; Yoo, W. J. Carrier Transport at the Metal-MoS2 Interface. *Nanoscale* **2015**, *7*, 9222−9228.
(37) Moodera, J.; Nowak, J.; van de Veerdonk, R. Interface Magnetism and Spin Wave Scattering in Ferromagnet-Insulator-Ferromagnet Tunnel Junctions. *Phys. Rev. Lett.* **1998**, *80*, 2941−2944.
(38) Das, S.; Appenzeller, J. Where Does the Current Flow in Two-Dimensional Layered Systems? *Nano Lett.* **2013**, *13*, 3396−3402.
(39) Sui, Y.; Appenzeller, J. Screening and Interlayer Coupling in Multilayer Graphene Field-Effect Transistors. *Nano Lett.* **2009**, *9*, 2973−2977.
(40) Yu, W. J.; Li, Z.; Zhou, H.; Chen, Y.; Wang, Y.; Huang, Y.; Duan, X. Vertically Stacked Multi-Heterostructures of Layered Materials for Logic Transistors and Complementary Inverters. *Nat. Mater.* **2013**, *12*, 246−252.
(41) Moriya, R.; Yamaguchi, T.; Inoue, Y.; Sata, Y.; Morikawa, S.; Masubuchi, S.; Machida, T. Influence of the Density of States of Graphene on the Transport Properties of graphene/MoS2/metal Vertical Field-Effect Transistors. *Appl. Phys. Lett.* **2015**, *106*, 223103.
(42) Sata, Y.; Moriya, R.; Morikawa, S.; Yabuki, N.; Masubuchi, S.; Machida, T. Electric Field Modulation of Schottky Barrier Height in graphene/MoSe2 van der Waals Heterointerface. *Appl. Phys. Lett.* **2015**, *107*, 23109.
(43) Julliere, M. Tunneling between Ferromagnetic Films. *Phys. Lett. A* **1975**, *54*, 225−226.
(44) Moodera, J. S.; Kinder, L. R.; Wong, T. M.; Meservey, R. Large Magnetoresistance at Room Temperature in Ferromagnetic Thin Film Tunnel Junctions. *Phys. Rev. Lett.* **1995**, *74*, 3273−3276.
(45) Tran, T. L. A.; Le, T. Q.; Sanderink, J. G. M.; Van Der Wiel, W. G.; De Jong, M. P. The Multistep Tunneling Analogue of Conductivity Mismatch in Organic Spin Valves. *Adv. Funct. Mater.* **2012**, *22*, 1180−1189.
(46) Xiao, D.; Liu, G. B.; Feng, W.; Xu, X.; Yao, W. Coupled Spin and Valley Physics in Monolayers of MoS 2 and Other Group-VI Dichalcogenides. *Phys. Rev. Lett.* **2012**, *108*, 196802.
(47) Xiong, Z. H.; Wu, D.; Vardeny, Z. V.; Shi, J. Giant Magnetoresistance in Organic Spin-Valves. *Nature* **2004**, *427*, 821−824.
(48) Park, B. G.; Banerjee, T.; Lodder, J. C.; Jansen, R. Tunnel Spin Polarization *versus* Energy for Clean and Doped Al2O3 Barriers. *Phys. Rev. Lett.* **2007**, *99*, 217206.
(49) Yuasa, S.; Nagahama, T.; Fukushima, A.; Suzuki, Y.; Ando, K. Giant Room-Temperature Magnetoresistance in Single-Crystal Fe/MgO/Fe Magnetic Tunnel Junctions. *Nat. Mater.* **2004**, *3*, 868−871.
(50) Shang, C.; Nowak, J.; Jansen, R.; Moodera, J. Temperature Dependence of Magnetoresistance and Surface Magnetization in Ferromagnetic Tunnel Junctions. *Phys. Rev. B: Condens. Matter Mater. Phys.* **1998**, *58*, 2917−2920.
(51) Coey, J. M. D. *Magnetism and Magnetic Materials*; Cambridge University Press, 2010; Vol. *12*.
(52) Rocha, A. R.; García-suárez, V. M.; Bailey, S. W.; Lambert, C. J.; Ferrer, J.; Sanvito, S. Towards Molecular Spintronics. *Nat. Mater.* **2005**, *4*, 335−339.
(53) Rocha, A. R.; García-Suárez, V. M.; Bailey, S.; Lambert, C.; Ferrer, J.; Sanvito, S. Spin and Molecular Electronics in Atomically Generated Orbital Landscapes. *Phys. Rev. B: Condens. Matter Mater. Phys.* **2006**, *73*, 085414.
(54) Rungger, I.; Sanvito, S. Algorithm for the Construction of Self-Energies for Electronic Transport Calculations Based on Singularity Elimination and Singular Value Decomposition. *Phys. Rev. B: Condens. Matter Mater. Phys.* **2008**, *78*, 035407.
(55) Soler, J. M.; Artacho, E.; Gale, J. D.; Garcia, A.; Junquera, J.; Ordejon, P.; Sanchez-Portal, D. The SIESTA Method for Ab Initio Order-N Materials Simulation. *J. Phys.: Condens. Matter* **2002**, *2745*, 22.
(56) Ceperley, D. M.; Alder, B. J. Ground State of the Electron Gas by a Stochastic Method. *Phys. Rev. Lett.* **1980**, *45*, 566−569.

DOI: 10.1021/acsnano.7b02819
ACS Nano 2017, 11, 6389−6395